Code-Carrier Divergence Monitoring for GAST-F GBAS

Yiping Jiang, Carl Milner, Christophe Macabiau

Code-Carrier Divergence Monitoring for GAST-F GBAS

Yiping Jiang[(1)], Carl Milner[(2)], Christophe Macabiau[(3)]
ENAC, Toulouse, France
jiang@recherche.enac.fr[(1)], milner@recherche.enac.fr[(2)], macabiau@recherche.enac.fr[(3)]

ABSTRACT

In Ground Based Augmentation System (GBAS), non Gaussian tails are created by ionosphere when detecting a satellite payload fault with the Code Carrier Divergence (CCD) ground monitor. Ionosphere can also trigger alarms which is not distinguishable with the payload fault. Using multi-frequency observations which would be available in future supporting GBAS Approach Service Type F (GAST-F), a new CCD monitor is proposed with influence of ionosphere removed. The improved performance is shown with the empirical data and simulated scenarios. The worst case is concluded for analysis of compliance with the integirty requirement.

1. INTRODUCTION

The GBAS is intended to support precision approach operations standardized at the International Civil Aviation Organization (ICAO) using satellite constellations. Single frequency based GBAS Approach Service Type D (GAST-D) is developed to transfer more responsibility from the ground station to the aircraft to reach CAT II/III minima. However, the GAST-D solution whilst meeting the requirements most of the time in most locations is susceptible to ionospheric activity at times in some locations. To take advantages of the forthcoming multi-constellation and multi-frequency GNSS environment, the GAST-F has been designated to the provision of CAT III services using dual-frequency corrections which will mitigate the issues raised under GAST-D, which is under investigation within the European SESAR program (WP 15.3.7). Furthermore, the enhanced performance of the navigation system should enable lower performing aircraft to meet the CAT III requirements.

In the design of GAST-F one aspect which may be revisited to garner better performance is the design of integrity monitors for the array of threats which constitute a risk to GBAS. These threats may differ when considering new signals and constellations. This paper addresses the monitoring of the CCD on the ground caused by a satellite payload fault, which results in a lack of synchronization between the code and carrier waveform during the data demodulation and processing and after the tracking loop by GNSS receivers [1]. The payload threat takes more arbitrary forms, which can occur on the code only or carrier only or both code and carrier. In GAST-D, multiple monitors act together to constrain the effect of this error on the ground and aircraft [2][3], including the CCD rate monitor [4], the excessive acceleration monitor [5] and the carrier rate monitor. In this study, only the CCD rate monitor is of concern. On detection of such failures, the associated range source shall be removed from the valid sets or indicated [6].

Nominal ionosphere at low elevation angle leads to non Gaussian tails of the test metrics. This is isolated by increasing the standard deviation of the metric noise resulting in a larger threshold. However, in case of the ionosphere, large temporal gradients can still trigger false alarms in the CCD monitor. The role of the ground CCD monitor is not designed to protect against ionosphere gradient because the slowly varying ionosphere gradient is cancelled in the differential processing and fast varying gradients are detected with airborne monitoring. With GAST-D multiple frequency measurements, it is possible to remove the ionosphere with resulting advantages as follows: 1) Without the ionosphere error in the residual noise in the test metrics, the standard deviation of the metric noise does not need to account for this effect, which could potentially enable the same performance to be obtained with less allocated continuity risk. 2) The two failure types of the ionosphere and the satellite payload CCD fault, which would both trigger alarms in the CCD monitor in GAST-D, is now distinguishable and only the latter one is detected by the ground CCD monitor.

The rest of the paper is organized as follows. Starting with an introduction of GAST-D CCD monitor, the design of the new GAST-F monitor is described with the covariance matrix bounded with empirical data. Then the divergence's influence on the airborne and ground smoothing process is analyzed and the worst case differential error with CCD detection is concluded for both GAST-D and GAST-F. Lastly, the results of the Probability of Missed Detection (PMD) as a function of the divergence and the differential error are used for compliance analysis, where the worst case mapping functions are obtained for GAST-D and GAST-F.

2. INTEGRITY MONITORS

2.1 GAST-D CCD Monitor

In GAST-D CCD Monitor, the Code minus Carrier (CMC) single frequency observations are used. With GPS L1 pseudorange ρ_1 and phase measurement φ_1 as an example,

$$CMC_1(t) = \rho_1(t) - \varphi_1(t) \tag{1}$$

With T as the sample interval, the CMC rate is defined as,

$$dCMC_1 = \frac{CMC_1(t) - CMC_1(t-T)}{T} \tag{2}$$

Thus errors common to code and carrier measurements, such as satellite and receiver clock offsets, troposphere delay, orbit and ephemeris error and etc. are eliminated. Constant errors are removed, e.g. the integer ambiguity. The difference between two epochs removes largely the slowly varying biases. The leftover errors appear in the form of rate of change of the ionosphere delay, multipath and noise. The two cascaded first order low pass filter f is defined as,

$$F_1(t) = (1-\alpha)F_1(t-T) + \alpha \cdot dCMC_1 \tag{3}$$

$$F_2(t) = (1-\alpha)F_2(t-T) + \alpha \cdot F_1(t) \tag{4}$$

where $dCMC_1$ is the input and $F_2(t) = f(dCMC_1)$ is the output of the filter, $\alpha = \frac{T}{\tau}$ is the filter weight with τ as the time constant. Shorter time constant results in faster detection of CCD failure, and therefore less susceptible to the buildup of divergence induced filter lag errors, but the noisier test metric. In s-domain, the test metric of GAST-D is expressed as,

$$F_2(s) = \frac{1}{(\tau s+1)^2} dCMC_1(s) = \frac{s}{(\tau s+1)^2} CMC_1(s) \tag{5}$$

For GAST-D, the non-centrality parameter of the test metric is the divergence rate d, and the steady state is the same which is independent of the time constant τ,

$$\lim_{s\to 0} sF_2(s) = \frac{s^2}{(\tau s+1)^2}\frac{d}{s^2} = d \tag{6}$$

In steady state, assuming the input noise is Gauss-Markov, the resulting noise attenuation is derived below when the filter weight is small,

$$\sigma_{F2}^2 \cong \frac{\alpha}{4}\sigma_{dCMC_1}^2 \tag{7}$$

For GAST-D, the continuity risk allocated for all monitors is 2×10^{-7} per 15s and satellite, and single monitor is 1/20, which is 10^{-8} per 15s and satellite [7]. The standard deviation of the test metric is bounded as 0.00399m/s, which is inflated to count for the fact that the ionosphere as one of the residual errors is not Gaussian (Simili and Pervan 2006). With the Probability of False Alarm (PFA) as 10^{-9}, the threshold is 0.0233m/s. The time constant on the ground is 30s [8]. For the Airborne CCD monitoring, the standard deviation of the test metric is 0.0022m/s, the threshold is 0.0125m/s [9], and the time constant is 100s [8]. This paper is only concerned with the CCD monitor on the ground.

2.2 GAST-F CCD Monitor

The ionospheric delay is eliminated by using multiple frequency measurements in GAST-F. As the starting point, the CCD caused by the payload fault is assumed to have an arbitrary form in GAST-F. If the satellite fault is originated from the oscillator only, the divergence rate magnitudes between two difference frequencies should be equal with the ratio of two frequencies. But if this is valid, the divergence in code and carrier measurements should also have a similar ratio in the single frequency GAST-D monitor. Since this was not assumed, the assumption of the ratio of two frequencies is also not accepted and arbitrary divergence rates are assumed.

Using GPS L1 and L5 or Galileo E1 and E5, four monitor statistics are used each with ionosphere removed, including the Divergence Free (DF) combination on L1, DF on L5, Ionosphere Free (IF) combination on CMC and IF on phase measurements,

$$CMC_{DF1} = \rho_1 - \varphi_1 + \frac{2}{1-\gamma}(\varphi_1 - \varphi_5) \tag{8}$$

$$CMC_{DF5} = \rho_5 - \varphi_5 - \frac{2\gamma}{\gamma-1}(\varphi_1 - \varphi_5) \tag{9}$$

$$CMC_{IF} = \frac{\gamma}{\gamma-1}(\rho_1 - \varphi_1) - \frac{1}{\gamma-1}(\rho_5 - \varphi_5) \tag{10}$$

$$\varphi_{IF} = \frac{\gamma}{\gamma-1}\varphi_1 - \frac{1}{\gamma-1}\varphi_5 \tag{11}$$

where $\gamma = \frac{f_{L1}^2}{f_{L5}^2}$. $dCMC_{DF1}$ is the CMC_{DF1} change rate between two adjacent epochs, which can also be expressed as a change rate of measurements $d\rho_1$, $d\rho_5$, $d\varphi_1$, $d\varphi_5$,

$$dCMC_{DF1} = \frac{CMC_{DF1}(t) - CMC_{DF1}(t-T)}{T} = d\rho_1 - d\varphi_1 + \frac{2}{1-\gamma}(d\varphi_1 - d\varphi_5) \tag{12}$$

Same can be derived for the change rate of the other three statistics $dCMC_{DF5}$, $dCMC_{IF}$ and $d\varphi_{IF}$. Since $d\varphi_{IF}$ is not geometry free, it needs to be compensated for satellite motion dr, receiver clock drift dt_{rx}, satellite clock drift dt_{sv} and also troposphere delay for low elevation angle satellites. The phase measurements need to be checked against cycle slips for all four monitor statistics. The receiver clock is estimated by averaging the rest of the geometry-free satellites $d\varphi_{IF,j}$ together,

$$dt_{rx,j} = \frac{1}{n}\sum_{j\neq i}(d\varphi_{IF,j} - dr_j - dt_{sv,j}) \tag{13}$$

where n is the number of visible satellites excluding the one that is examined of the CCD. The compensated IF phase statistic becomes

$$d\varphi_{IF\_C} = d\varphi_{IF,i} - dr_i - dt_{sv,i} - dt_{rx,i} \tag{14}$$

To cover arbitrary fault modes on code, carrier, L1 and L5, the only and unique solution to make the mean of each of the four statistics $dCMC_{DF5}$, $dCMC_{DF5}$, $dCMC_{IF}$, $d\varphi_{IF\_C}$ equals zero at the same time is when the mean of each measurement rate $d\rho_1, d\rho_5, d\varphi_1, d\varphi_5$ is zero. With four statistics going through the same second-order filter f as in GAST-D, the filtered statistics are $f(dCMC_{DF5})$, $f(dCMC_{DF5}), f(dCMC_{IF})$, $f(d\varphi_{IF\_C})$. Define a vector $x = [f(dCMC_{DF1})\ f(dCMC_{DF5})\ f(dCMC_{IF})\ f(d\varphi_{IF\_C})]$, the quadratic form is used as the GAST-F test metric,

$$D_F = xQ^{-1}x^T \tag{15}$$

where Q is the covariance matrix of vector x. Assuming there is no temporal correlation on all measurements, the covariance matrix Q is given by,

$$\begin{aligned}
Q(1,1) &= \frac{\alpha}{4T^2}(2\sigma_{\rho1}^2 + 24.9\sigma_{\varphi1}^2 + 12.8\sigma_{\varphi5}^2); & Q(2,2) &= \frac{\alpha}{4T^2}(2\sigma_{\rho5}^2 + 41.0\sigma_{\varphi1}^2 + 24.9\sigma_{\varphi5}^2)\\
Q(3,3) &= \frac{\alpha}{4T^2}(10.2\sigma_{\rho1}^2 + 3.2\sigma_{\rho5}^2 + 10.2\sigma_{\varphi1}^2 + 3.2\sigma_{\varphi5}^2); & Q(4,4) &= \frac{\alpha}{4T^2}(10.2\sigma_{\varphi_1}^2 + 3.2\sigma_{\varphi_5}^2 + \frac{10.2\sigma_{\varphi_1}^2}{n} + \frac{3.2\sigma_{\varphi_5}^2}{n})\\
Q(1,2) &= \frac{\alpha}{4T^2}(32\sigma_{\varphi1}^2 + 17.9\sigma_{\varphi5}^2); & Q(1,3) &= \frac{\alpha}{4T^2}(4.52\sigma_{\rho1}^2 + 15.9\sigma_{\varphi1}^2 + 6.4\sigma_{\varphi5}^2)\\
Q(1,4) &= \frac{\alpha}{4T^2}(-15.9\sigma_{\varphi1}^2 - 6.4\sigma_{\varphi5}^2); & Q(2,3) &= \frac{\alpha}{4T^2}(-2.5\sigma_{\rho5}^2 + 20.5\sigma_{\varphi1}^2 + 8.9\sigma_{\varphi5}^2)\\
Q(2,4) &= \frac{\alpha}{4T^2}(-20.5\sigma_{\varphi1}^2 - 8.9\sigma_{\varphi5}^2); & Q(3,4) &= \frac{\alpha}{4T^2}(-2.26\sigma_{\varphi1}^2 - 3.2\sigma_{\varphi5}^2)
\end{aligned} \tag{16}$$

After averaging with multiple ground stations in GBAS, the covariance is further reduced as Q/M with M as the number of ground stations. Assuming the noise of ρ_1, ρ_5, φ_1, φ_5 are Gaussian, with the Cholesky decomposition of Q, the four statistics in vector x are standardized and decorrelated, and therefore the test metric is of chi-squared distribution with 4 degrees of freedom.

For GAST-F, the fault mode is defined by the location with measurements including carrier only, code only, and carrier code, and with frequency including L1 only, L5 only or both L1 and L5. Therefore, there are totally 15 fault modes: "Code L1", "Code L5", "Carrier L1", "Carrier L5", "Code L1+L5", "Carrier L1+L5", "Code+Carrier L1", "Code+Carrier L5", "Code L1, Carrier L5", "Code L5, Carrier L1", "Code L1+L5, Carrier L1", "Code L1+L5, Carrier L5", "Code L1, Carrier L1+L5", "Code L5, Carrier L1+L5" and "Code+Carrier L1+L5". Assume the divergence rate on Code L1 as $d1_C$, Carrier L1 as $d1_L$, Code L5 as $d5_C$, Carrier L5 as $d5_L$, the rate shows the same value in the steady state non-centrality parameter of the test metric as proved in (6). For example, the statistic $dCMC_{DF1}$ in the test metric has steady state non-centrality parameter as $d1_C - d1_L + \frac{2}{1-\gamma}(d1_L - d5_L) = d1_C - 3.53d1_L + 2.53d5_L$. Therefore, the non-centrality parameter of the steady state test metric is $\delta = C_x^T Q^{-1} C_x$ with C_x,

$$C_x = \begin{bmatrix} d1_C - 3.53d1_L + 2.53d5_L \\ d5_C - 4.53d1_L + 3.53d5_L \\ 2.26(d1_C - d1_L) - 1.26(d5_C - d5_L) \\ 2.26d1_L - 1.26d5_L \end{bmatrix} \tag{17}$$

3. OVERBOUNDING WITH EMPIRICAL DATA

The 1Hz data collected in Pattonville with a MLA antenna is used to bound the test metric provided by Thales Electronic Systems. The elevation mask is 5° and the filter output is only used 360s after initialization. The time constant is 30s. There are totally 8 GPS satellites with both L1 and L5 during one day.

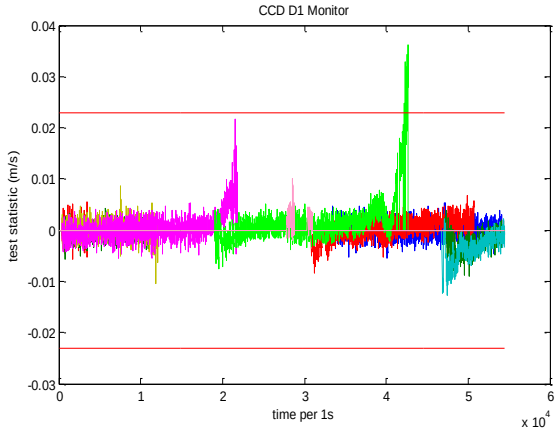

Fig. 1. GAST-D L1 CCD Monitor

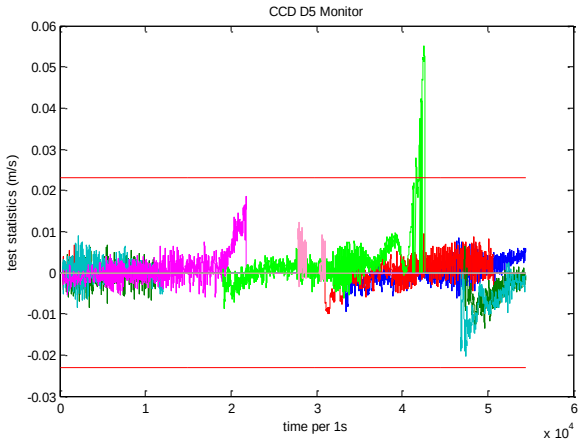

Fig. 2. L5 CCD Monitor

With the threshold set as 0.023m/s in GAST-D, there is a false alarm triggered in both Fig. 1 and Fig. 2 with SV27 due to ionosphere delay at low elevation angle, which can be avoided with the new DF and IF combinations. Two of the four statistics in the new GAST-F test metric are shown in Fig. 3 and Fig. 4 as the DF on L1 and L5.

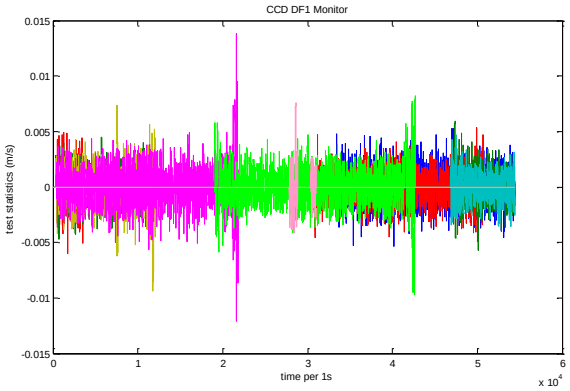

Fig. 3. GAST-F DF1 CCD Monitor

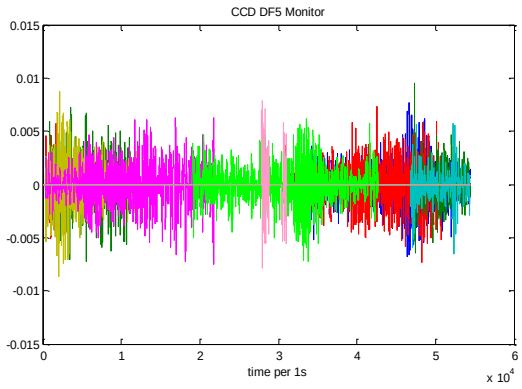

Fig. 4. GAST-F DF5 CCD Monitor

The standard deviation of six statistics before and after filtering are shown in Table 2 with $dCMC_5$ as the CMC rate on L5,

Table 2. Standard Deviation of 6 Statistics before and after Filtering

Before	$dCMC_1$	$dCMC_5$	$dCMC_{DF1}$	$dCMC_{DF5}$	$dCMC_{IF}$	$d\varphi_{IF\_C}$
(m)	0.1451	0.0456	0.1451	0.0458	0.1451	0.0163
After	f($dCMC_1$)	f($dCMC_5$)	f($dCMC_{DF1}$)	f($dCMC_{DF5}$)	$f(dCMC_{IF})$	$f(d\varphi_{IF\_C})$
(m)	0.0032	0.0055	0.0012	0.0012	0.0031	0.00085

With (7), the results after filtering should be 1/120 of the results before filtering. But the results in practice does not exactly coincide with this conclusion, which is caused by the discrepancy with the assumption of pure Gaussian-Markov. The filter reduced fast varying error, while the slow varying part is relatively kept. Since the leftover low frequency part causes stronger correlation between L1 and L5, such as the ionosphere error in f($dCMC_1$) and f($dCMC_5$), the correlation is not negligible. The bounded covariance of the test metric with empirical data is,

$$Q = \begin{bmatrix} 0.1484 & & & \\ 0.0001 & 0.1356 & & \\ 0.3353 & -0.1709 & 0.9735 & \\ 0.0003 & 0.0004 & 0 & 0.0724 \end{bmatrix} \times 10^{-5} \tag{18}$$

4. THE WORST CASE DIFFERENTIAL ERROR

In GBAS, both the ground station and airborne user smooth the raw pseudoranges with a Hatch filter,

$$\hat{\rho}(t) = \alpha\rho(t) + (1-\alpha)[\hat{\rho}(t-T) + \varphi(t) - \varphi(t-T)] \tag{19}$$

where $\hat{\rho}$ is the smoothed pseudorange, ρ is the raw pseudorange, φ is the raw phase measurement, $\alpha_s = \frac{T}{\tau_s}$ is the smoothing filter weight and τ_s is the time constant. There is an introduced 30s smoothed pseudorange in GAST-D in addition to the original 100s time constant. Besides monitoring the GNSS signals, the GBAS ground station transmits differential corrections via a VHF Data Broadcast (VDB) every 0.5s. Among the broadcast information, pseudorange corrections (PRC) and range rate correction (RRC) are computed with ground smoothed pseudoranges, which are used by airborne to calculate the differential pseudorange ρ_c,

$$\rho_c = \hat{\rho} + PRC + RRC(t - t_z) + TC + c\Delta t_{sv} \tag{20}$$

where $\hat{\rho}$ is the airborne carrier smoothed pseudorange, t_z is the time of application of PRC, TC is the tropospheric correction and Δt_{sv} is the satellite clock correction from the navigation message. The characteristics of the differential error is analyzed first without detection and then together with the CCD monitor in this section. Since the filter is continuous in time, the smoothed pseudorange $C(s)$ can be expressed in Laplace domain.

$$C(s) = \frac{1}{\tau s+1}c(s) + \frac{\tau s}{\tau s+1}p(s) \tag{21}$$

where $c(s)$ and $p(s)$ are the raw pseudorange and phase measurements in Laplace domain. Assume the divergence is a ramp error with the divergence rate in code only as d_C, phase only as d_L and both code and phase as $d_C - d_L$, the smoothed range error only has steady state $d_L\tau$ when divergence is in phase only. This is derived by

$$\lim_{s\to 0} sC(s) = \lim_{s\to 0}\left(\frac{s}{\tau s+1}\cdot\frac{d_C}{s^2} + \frac{\tau s^2}{\tau s+1}\cdot\frac{d_L}{s^2}\right) \tag{22}$$

The rate of the smoothed range error has steady state of d_C, 0 and d_C for code only, phase only and both code and phase respectively, which is derived by,

$$\lim_{s\to 0} s[sC(s) - C(0)] = \lim_{s\to 0}\left(\frac{s^2}{\tau s+1}\cdot\frac{d_C}{s^2} + \frac{\tau s^3}{\tau s+1}\cdot\frac{d_L}{s^2}\right) \tag{23}$$

Therefore, the steady state of the smoothed error is related with time constant τ when divergence is in phase only. With differencing the smoothed pseudorange from the ground and airborne filters, the differential range is subsequently

influenced by the divergence magnitude, the fault onset time t_f, the ground filter initializing time t_g, the airborne filter initializing time t_a and the time delay from initialization of the airborne filter to incorporation of the measurement in position solution t_{delay}.

The GAST-D results of the 30s smoothed error and the 30s differential error E_r without detection are shown in Fig. 5 with the worst case when the ground filter is initialized 360s before fault onset, and the airborne filter is initialized at the same time with the fault onset. For GAST-F, there are two smoothing filter for L1 measurements and L5 measurements respectively. The airborne smoothing filter can have *variant* time constant or *invariant* time constant. For the variant time constant, with time t from filter initialization for duration of τ, $[0\sim\tau]$, the time constant is variant as t. After this, the time constant is also constant as τ, which is the same as the ground time constant. In this simulation, the random error is neglected, the divergence magnitude is 0.01m/s for "Code" only, -0.01m/s for "Carrier" only and both 0.01m/s and -0.01m/s for "Code-Carrier", and $T = 0.5s$.

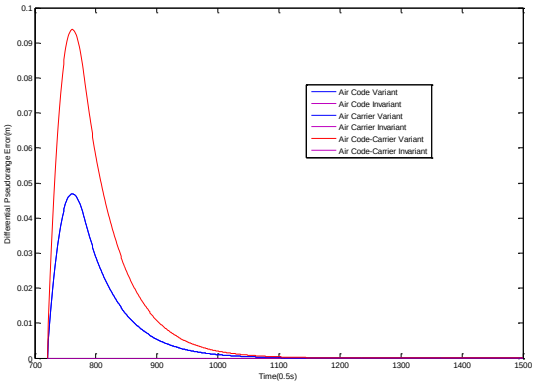

Fig. 5. GAST-D Differential Error

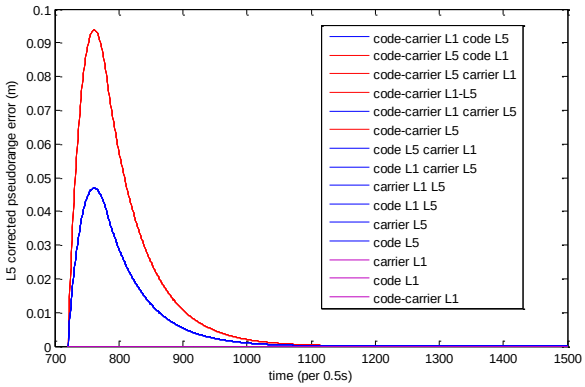

Fig. 6. GAST-F L5 Differential Error with Variant Filter

In Fig. 5, when both air and ground filter are stabilized, the differential error is zero. During the transient state, all "Invariant" results are zero, and "Code Variant" is the same as "Carrier Variant", which are half the magnitude of "Code-Carrier Variant". This can be explained by the expanded equation of the differential smoothed error. A key parameter is the delay to incorporation in airborne solution t_{delay}. The maximum differential range error with "Carrier Variant" as a function of t_{delay} and $t_a - t_f$ is shown below. With the GAST-D CCD monitor and threshold set as 0.0233m/s, the detected measurements are removed out of the ground and airborne smoothing filter. With delay to incorporation as 50s, the value of which is proposed to be standardized, the maximum differential error as a function of the divergence rate magnitude and the airborne initialization relative to fault onset are in Table 3.

Table 3 GAST-D Maximum Differential Error with t_{delay}=50s

Failure Source	*Carrier Variant*	*Carrier Invariant*	*Code Variant*	*Code Invariant*	*Code+Carrier Variant*	*Code+Carrier Invariant*
Max(Er)(m)	0.1745	0.1142	0.1763	0.1142	0.1524	0.111
Div.(m/s)	0.04	0.04	0.04	0.04	0.02	0.02
$t_a - t_f$ *(s)*	35	35	35	35	-150	-150

In Fig. 6, the GAST-F differential error have similar characteristics with the GAST-D results, where "Code" is the same as "Carrier", which are half the magnitude of "Code-Carrier".All failures happened on L1 obviously does not have effect on the L5 differential error. For the differential error with detection, the GAST-F CCD monitor is not able to distinguish if there is failure on L1 or L5, so the measurements are removed out of the ground and airborne L1 and L5 smoothing filter when there is any failure on L1 or L5. With bounded covariance matrix and PFA set as 10^{-9}, the threshold is 47.8795 $(m/s)^2$. The worst case differential error with detection as a function of the divergence rate magnitude and the airborne initialization relative to fault onset is listed in Table 4 with L5 as an example,

Table 4 GAST-F L5 Maximum Differential Error with t_{delay}=50s

Failure Source	*Code L5 Variant*	*Carrier L5 Variant*	*Code+Carrier L5, Variant*
Max(Er)(m)	0.0625	7.153×10^{-6}	2.302×10^{-4}

Div.(m/s)	0.02	0.02	0.02
$t_a - t_f$ *(s)*	-41	28	25

5. THE PMD AS A FUNCTION OF THE DIFFERENTIAL ERROR

First, the projection from the divergence domain d and the non-centrality parameter δ in the test metric domain needs to be examined. The ratio of d and δ is always unit in GAST-D no matter if the divergence is code only, carrier only or both code and carrier. However, with the new non-linear monitor in GAST-F, this ratio not constant as shown in Fig. 7 for all fault modes with divergence in code the same as the x-axis d and divergence in carrier as $-d$, and the same value is assumed on L1 and L5. The GAST-D is not shown in Fig. 7, whose ratio is much smaller than all GAST-F ratios. As shown in Fig. 7, with the same divergence magnitude, some fault modes would produce bigger non-centrality parameter, making it easier to detect the failure, including "Code-Carrier L1 Code L5", "Carrier L1 Code L5", "Code-Carrier L1" and "Carrier L1". Consequently, this ratio influences the PMD performance as a function of the divergence magnitude with given threshold. As shown in Fig. 8, the modes with bigger ratios in Fig. 7 have better PMD performance.

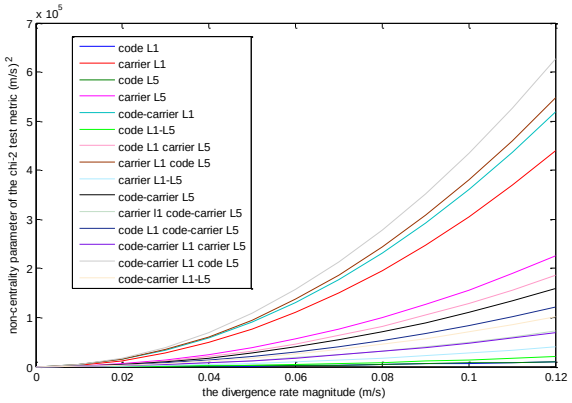

Fig. 7. GAST-F Non-centrality Parameter as a function of d

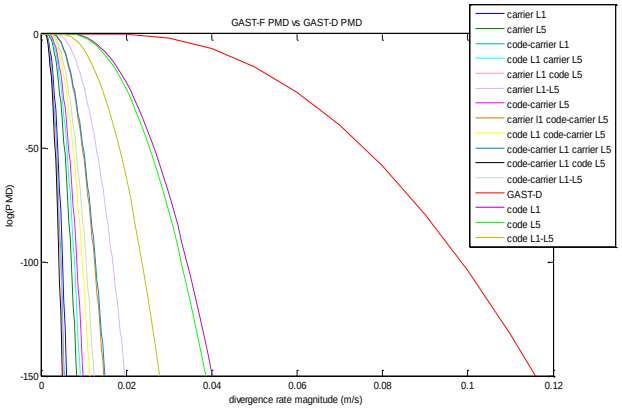

Fig. 8. GAST-D and GAST-F PMD as a function of d

The PMD required region is defined as a function of the differential error illustrated by the blue line in Fig. 9 and Fig. 10 [8]. Therefore, the *mapping function* defined as the ratio of the non-centrality parameter of the test metric δ and the differential error Er with unit 1/s needs to be studied. The PMD as a function of the test metric can be expressed as PMD as a function of Er with a given mapping function.

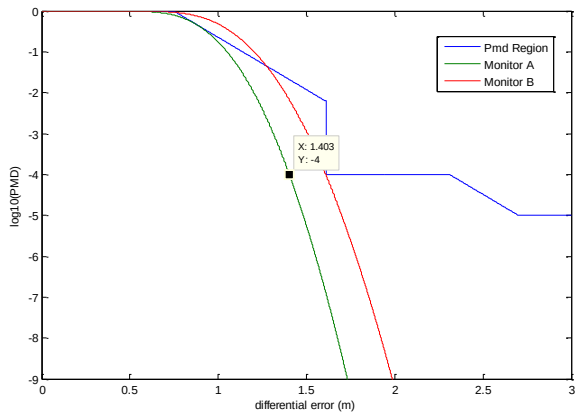

Fig. 9. GAST-D PMD Compliance

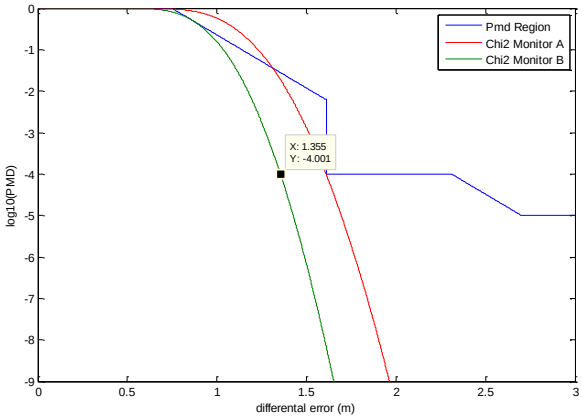

Fig. 10. GAST-F PMD Compliance

For GAST-D in Fig. 9, the green line is the worst case that is able to fulfil the requirement with normal distribution, which is derived by assuming that the mapping function is 0.0276 (1/s) with PFA as 10^{-9} and standard deviation of the test metric 0.00399m/s. For the GAST-F monitor in Fig. 10, the green line is also the worst case that is able to meet PMD requirements, which is derived by multiplying the non-centrality parameter by 56.6294. If the mapping function is bigger than 0.0276 (1/s) in GAST-D, which is defined as *the critical mapping function*, the PMD requirement can be satisfied. Similarly, the 56.6294 ($1/s^2$) is the critical mapping function in GAST-F. The worst case mapping function as a function

of the divergence rate and the airborne initialization time vs. fault onset with delay to incorporation as 50s are shown in Table 5 and Table 6.

Table 5. GAST-D Minimum Mapping Function with t_{delay}=50s

Failure Source	*Carrier Variant*	*Carrier Invariant*	*Code Variant*	*Code Invariant*	*Code+Carrier Variant*	*Code+Carrier Invariant*
Min(|f|)(1/s)	0.1299	0.1784	0.1300	0.1784	0.1663	0.4386
Div.(m/s)	0.03	0.02	0.02	0.02	0.02	0.03
$t_a - t_f$ *(s)*	-147	-149	-150	-150	-11	-8

Table 6. GAST-F Minimum Mapping Function with L5 smoothing and t_{delay}=50s

Failure Source	*Code L5 Variant*	*Carrier L5 Variant*	*Code+Carrier L5, Variant*
Min(|f|)(1/s^2)	70.795	1745.8	316.23
Div.(m/s)	0.02	0.002	0.003
$t_a - t_f$ *(s)*	-10	-57	-56

With all results bigger than the critical mapping function, the PMD compliance of GAST-D and GAST-F can be concluded. Also, comparing Table 3 and Table 5, the worst case differential range error does not happen at the same condition with the worst case mapping function, and the latter one should be defined as the real worst case in context of PMD compliance.

6. CONCLUSIONS

A new GAST-F CCD monitor is designed and demonstrated under the original GAST-D framework. The advantages of removing the ionosphere is shown with empirical data. With only eight satellites transmitting on the L5 frequency, the application of IF carrier combinations has difficulty to obtain enough satellites to remove the receiver clock with high precision, and therefore reducing availability. But this problem will be relieved as more L5 satellites are available.

ACKNOWLEDGMENTS

The authors would like to thank Thales Electronic Systems for the provision of data and partners of the SESAR WP 15.3.7. We would also like to thank Frieder Beck and Morten Stakkelan for their help and advices. This study is based on work supported by SESAR Joint Undertaking, created by ENAC, DSNA and Thales Electronic Systems within the frame of the SESAR Programme co-financed by the EU and EUROCONTROL. Any opinions, findings, or conclusions expressed in this study are those of the authors and do not necessarily reflect those of the SESAR Joint Undertaking.

References

[1] Gleason S. and Gebre-Egziabher, GNSS Applications and Methods, Artech House, 2009.

[2] Brenner, M. and Liu, F., Ranging Source Fault Detection Performance for Category III GBAS, Proceedings of the 23rd International Technical Meeting of the Satellite Division of the Institute of Navigation, Portland, OR, September 2010, pp. 2618-2632.

[3] Jensen D., Brenner M. & Murphy T., ICAO NSP - Preliminary Ground System Monitor Validation Results, 2009.

[4] Simili, D. V. and Pervan, B., Code-Carrier Divergence Monitoring for the GPS Local Area Augmentation System, Proceedings of IEEE/ION PLANS, 2006.

[5] Stakkeland M., Andalsvik Y., Jacobsen K., Estimating satellite excessive acceleration in the presence of phase scintillations, ION GNSS 2014.

[6] ED-114A, Minimum Operational Performance Specification for Global Navigation Satellite Ground Based Augmentation System Ground Equipment to Support Category I Operations, 2013.

[7] SARPs, GBAS CAT II/III Development Baseline SARPs, 2010.

[8] ICAO NSP, WGW/Flimsy 6 – Conceptual Framework for the Proposal for GBAS to Support CAT III Operations, 2009

[9] RTCA DO-253C, Minimum Operational Performance Standards for GPS Local Area Augmentation System Airborne Equipment, 2008.